Rock and Soil Mechanics

Volume 42 | Issue 12 Article 5

2-28-2022

Failure and instability mechanism of anchored surrounding rock for deep chamber group with super-large section under dynamic disturbances

Xue-sheng LIU
College of Energy and Mining Engineering, Shandong University of Science and Technology, Qingdao, Shandong 266590, China;

De-yuan FAN
College of Energy and Mining Engineering, Shandong University of Science and Technology, Qingdao, Shandong 266590, China;, deyuan926@126.com

Yun-liang TAN
College of Energy and Mining Engineering, Shandong University of Science and Technology, Qingdao, Shandong 266590, China;

Xin WANG
College of Energy and Mining Engineering, Shandong University of Science and Technology, Qingdao, Shandong 266590, China;

See next page for additional authors

Failure and instability mechanism of anchored surrounding rock for deep chamber group with super-large section under dynamic disturbances

Authors

Xue-sheng LIU, De-yuan FAN, Yun-liang TAN, Xin WANG, and Agafangelovich ALEXEY

Rock and Soil Mechanics 2021 42(12): 3407−3418 ISSN 1000−7598
https: //doi.org/10.16285/j.rsm.2021.5555 rocksoilmech.researchcommons.org/journal

Failure and instability mechanism of anchored surrounding rock for deep chamber group with super-large section under dynamic disturbances

LIU Xue-sheng[1, 2], FAN De-yuan[1, 2], TAN Yun-liang[1, 2], WANG Xin[1, 2], ALEXEY Agafangelovich[3]

1. State Key Laboratory of Mining Disaster Prevention and Control Co-founded by Shandong Province and the Ministry of Science and Technology, Shandong University of Science and Technology, Qingdao, Shandong 266590, China

2. College of Energy and Mining Engineering, Shandong University of Science and Technology, Qingdao, Shandong 266590, China; 3. College of Mining and Mechatronics, Kuzbass State Technical University, Kemerovo 650000, Russia

Abstract: The interaction of super-large section chamber group in deep and close-distance condition will lead to stress concentration and wide failure range of surrounding rock, especially under dynamic disturbances. In this paper, numerical simulation software FLAC3D is used to establish the calculation model based on the field condition of coal gangue separation system in Longgu Coal Mine. The deformation and failure evolution of chamber group under different chamber spacing and dynamic loads are studied by using built-in dynamic module. The simulation results show that: With the decrease of chamber spacing, the deformation and failure degree of surrounding rock gradually increases, and the overall failure and instability occur eventually. Compared with the static load, the range of critical spacing under dynamic disturbance is enlarged by 33.3%−50%. Meanwhile, the response of anchored surrounding rock is gradually intensified with the dynamic load strength increase, and the critical strength of failure and instability is about 4.0−4.5 MPa. Based on the elastic-plastic mechanics and elastic wave theories, the mechanical model of anchored surrounding rock under dynamic and static loads is established. The failure and instability criterion are obtained. The anchored surrounding rock can be divided into three states: overall stability, static failure and dynamic failure. On this basis, the analytical expression of critical distance between failure and instability is presented. Finally, in-site calculation and field monitoring verify the rationality and feasibility of the theoretical analysis. This study provides a reference for layout design and stability control of super-large section chamber group.

Keywords: dynamic disturbance; super-large section; chamber group; deformation and failure; instability

1 Introduction

In recent years, more and more large and super-large section chambers and chamber groups have been put into underground coal mine production in order to meet the requirements of intelligent and automatic construction for coal mines and green mining policy of gangue-not-lifting[1−3]. As the section area of the chamber increases, the stress concentration and deformation failure of surrounding rock is exacerbated significantly, and the control difficulty multiplies[4−6]. In addition, there are many large cross-section chambers in the underground coal mine distributed in groups. The surrounding rock stress is superimposed when the distance is close, resulting in the expansion of the failure range. Once a large rib spalling or roof collapse occurs in a certain chamber, it very likely incurs chain instability accidents. Especially in the process of deep mining, the frequency and intensity of dynamic load disturbance caused by blasting, rock burst, large area thick hard roof fracture and collapse, large machinery operation increase obviously, making the failure evolution of coal and rock mass more complex. The failure and instability of surrounding rock of super-large section chamber groups has become one of the main bottlenecks for safe and efficient mining in many mining areas in China[7−10].

At present, a great deal of research has been carried out on the evolution of deformation and failure, and instability mechanisms of chamber under dynamic disturbance. Based on the stress source of the dynamic disasters, the occurrence principle in chamber surrounding rock can be divided into three categories, namely, the high static load induced by the superposition of dynamic and static load, strong dynamic load, and low critical stress state[11−13]. On this basis, fruitful occurrence mechanisms of chamber surrounding rock dynamic disasters have been proposed, such as energy theory[14], strength theory[15], instability theory[16] and elastic wave theory[17]. Wang et al.[18] discussed the dynamic mechanism of rockburst induced by disturbance and surrounding rock structure, and proposed the principle and key technology of rockburst dynamic and static combined support, considering the

Received: 14 April 2021 Revised: 20 July 2021
This work was supported by the National Key R&D Program of China(2018YFC0604703).
First author: LIU Xue-sheng, male, born in 1988, PhD, Associate Professor, mainly engaged in the research on mining pressure and strata control. E-mail: xuesheng1134@163.com
Corresponding author: FAN De-yuan, male, born in 1994, PhD candidate, focusing on rock mechanics in mines. E-mail: deyuan926@126.com

structural effect of surrounding rock. Liu[19] established an energy-driven instability model of chamber surrounding rock under dynamic load, and expounded the occurrence mechanism of rockburst induced by dynamic load. Similar material simulation test is one of the important means to study the failure evolution of chamber surrounding rock under dynamic disturbance[20−21]. Using digital speckle technology, Pan et al.[22] carried out the similar simulation test of explosion loading and obtained the chamber dynamic failure process under explosion loading. Wang et al.[23] studied the deformation and failure response of surrounding rock under the combined action of dynamic and static loads by using large-scale geomechanical model test system. Zuo et al.[24] carried out dynamic and static combined loading tests on deep chamber gypsum model on Instron electro-hydraulic servo material testing machine, revealing the zonal fracture mechanism of surrounding rock of high stress chamber disturbed by dynamic load. By using numerical simulation methods, scholars studied the rule of chamber impact instability under different burial depths[25], lateral pressure coefficient[26], surrounding rock lithology[27], dynamic load strength[28] and other conditions, and obtained the stress distribution and deformation failure rule of surrounding rock in specific geological and mining situations.

In view of the practical issue of frequent surrounding rock instability accidents triggered by the interaction between close-distance underground chamber groups, current research focuses on the deformation and failure characteristics of surrounding rock, the influencing factors of rock stability and the control technology of surrounding rock[29−31]. Kang[32] explored the stress distribution characteristics of chamber surrounding rock and proposed the stability control countermeasures. By using numerical simulation, He et al.[33] found that the excavation of chamber group is a nonlinear irreversible process closely related to the stress path and stress history. Yang et al.[34] studied the chamber group of belt conveyor head in Zhaozhuang Coal Mine by means of field test and numerical simulation, and pointed out that the large section of the chamber, the low strength of surrounding rock, and the small width of coal pillar are the principal causes for the serious deformation and failure of chamber group. Wang et al.[35] described the influence of fault structure, horizontal stress and suction well excavation on the stability of chamber group surrounding rock.

To sum up, the existing studies mainly used on-site monitoring and numerical simulation approaches to investigate and calculate for specific geological and mining scenarios. Some valuable research results provided strong support for chamber support and surrounding rock control under specific conditions. However, at present, a more in-depth understanding of the new fracture evolution law and instability mechanism of surrounding rock under the complex condition of “deep+super-large section + close-distance chamber group” has not been formed. Therefore, taking the super-large section chamber group of the level −800 m coal gangue separation system in Longgu Coal Mine as the research background, the surrounding rock failure evolution of super-large section close-distance chamber group under different chamber spacings and dynamic loads was studied by using numerical simulation method. On this basis, an anchorage mechanical model of the chamber surrounding rock under dynamic and static combined loads was established to explore the failure and instability mechanism of the surrounding rock under dynamic load, and the field verification was also performed to provide a theoretical reference for the stability control of similar chamber surrounding rock.

2 Deformation and failure of anchored surrounding rock of chamber group

2.1 Numerical modeling

According to the actual geological condition of the gangue separation system in Longgu Coal Mine, two chambers (screening product transferring chamber(SPTC) and slime water and medium chamber (SWMC)) arranged across layers along the strike of coal seam are selected as research objects. The two chambers are 813 m in depth and have straight wall and semicircular arch. The spacing between them is 15−41 m, and the excavation length is 90 m and 93 m, respectively, as shown in Fig.1. The fuzzy comprehensive clustering discrimination indicates that both chambers belong to super-large section chambers[1]. The primary support of the chambers is bolt and cable combined support, using Φ22 mm×2 500 mm-MSGLW-600 rebar resin bolt without longitudinal rib, 200 mm× 200 mm×10 mm-Q235 high convex angle steel saucer, Φ22 mm×6 300 m-SKL18-1/1860 steel strand cable. The spacing between the bolts is 1 000 mm×1 000 mm, the chambers roof is installed by 5 anchor cables, the center cable is located in the center of the roof, and the interval between the cables on both sides and the center cable is 1 850 mm. The first cable is placed 1 300 mm down from the roof, and the second anchor cable is placed 3 000 mm

apart. The two sides of the chambers are installed by two rows of cable at an interval of 3 000 mm.

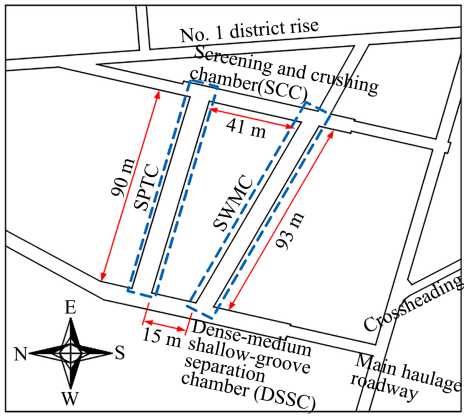

Fig. 1 Layout of coal gangue separation system

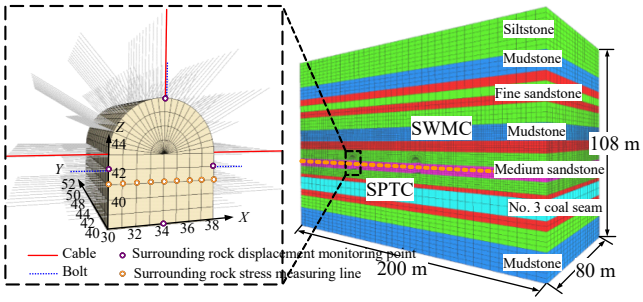

Fig. 2 Numerical simulation model and arrangement of measuring points

The numerical model (length × width × height = 200 m×80 m×108 m) was developed in FLAC3D. The shape and size of the chamber section were set according to the actual working conditions. The numerical model was divided into 1 071 153 units and 1 056 704 nodes, as shown in Fig.2. Mohr-Coulomb constitutive model was adopted in the model. Mechanical parameters of coal seam, roof and floor rock were summarized in Table 1.

Table 1 Mechanical properties of coal and rock[36]

Lithology	Density /(kg • m^{-3})	Bulk modulus /GPa	Shear modulus /GPa	Cohesion /MPa	Internal friction angle /(°)	Tensile strength /MPa
Siltstone	2 630	5.40	2.70	1.50	36.0	1.15
Mudstone	2 210	2.56	1.72	1.25	30.0	1.58
Fine sandstone	2 540	5.56	4.17	2.00	32.5	2.50
No. 3 coal seam	1 400	1.30	1.02	1.10	28.5	0.50
Medium sandstone	2 580	5.82	3.69	2.40	34.0	2.00

Model boundary conditions: During the static calculation, horizontal hinge constraints are imposed on the left and right boundaries of the model. The bottom boundary is fixed, and the top boundary is free and bears vertical stress equivalent to the overburden weight. The overburden load is calculated as $q = \gamma H$, which is 18.7 MPa, where γ refers to the average volumetric weight of overburden, 2.5×10^4 N /m^3, and H is the thickness of overburden (m). In the process of dynamic calculation, static boundary is adopted at the bottom and top, and free field boundary is applied at the front, back, left and right to realize the infinite field modeling. In addition, the dynamic multi-step method is used to classify the elements and nodes in the model to reduce the time required for dynamic calculation.

Simulation scheme: Six spacing simulation schemes (40, 30, 25, 20, 15, and 10 m) are set, respectively. According to the on-site chamber excavation sequence, the SPTC and SWMC are excavated successively in the model predetermined position, and a dynamic load of 2.0 MPa is applied to each model to calculate to the equilibrium state. Then, according to the spacing simulation results, the critical chamber spacing is selected to further explore the deformation and failure characteristics of surrounding rock under different dynamic load strengths. Six dynamic load strengths are set up, which are 2.5, 3.0, 3.5, 4.0, 4.5, and 5.0 MPa, respectively.

Support scheme: According to the actual form of underground support, the two chambers in the model adopt bolt and cable combined support. The bolt and cable are modeled by “Cable” unit in “Structural Elements”, and they are decomposed into 24 and 62 element, respectively. The length of each element is 0.1 m. In the anchoring section, spring element and friction element are used in series to interact with the hole wall element. In the free section, spring element is used to simulate the preload. The exposed end is rigidly connected with the roof element node. Mechanical parameters of bolt (cable) are listed in Table 2.

Table 2 Mechanical properties of bolts and cables[37]

Support structure	Density /(kg • m^{-3})	Elasticity modulus /GPa	Yield strength /MPa	Ultimate strength /MPa	Preload /kN
Bolt	6 000	200	500	700	100
Cable	4 500	195	1 720	1 860	150

Application of dynamic load: The built-in Dynamic module of the software is used for dynamic calculation, and Rayleigh damping is introduced to weaken the natural vibration of the system[38]. According to the field monitoring results, it is found that the dynamic load occurs frequently in the range of 0−100 m above the coal seam, with the intensity ranges from 2.0−5.0 MPa. Therefore, a dynamic

load disturbance is applied to the overlying strata located at a vertical distance of 60 m above the roof. The disturbance waveform is a sinusoidal wave with a frequency of 20 Hz. The time cycle of the dynamic load is 0.05 s.

Arrangement of monitoring points: (1) The stress measuring line is set 3 m above the bottom of the chamber, and the stress monitoring points are arranged every 1 m to record the stress variation of the anchored surrounding rock in this area. (2) The displacement monitoring points are set at the top and bottom of the screening product transfer chamber and the center of the two sides to monitor the roof-to-floor displacement and two sides deformation evolution.

2.2 Deformation and fracture law of surrounding rock

2.2.1 Chamber spacing

Under the influence of excavation and dynamic disturbance, the stress distribution of anchored surrounding rock of super-large section chamber group under dynamic and static loads is displayed in Fig.3, and the deformation of the roof, floor and two sides are shown in Fig.4. Part of plastic failure zones are shown in Fig.5.

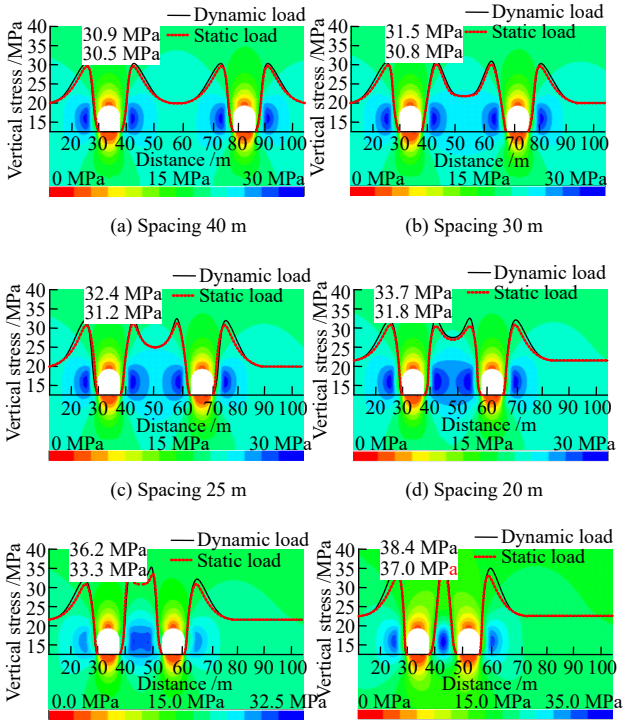

(a) Spacing 40 m (b) Spacing 30 m

(c) Spacing 25 m (d) Spacing 20 m

(e) Spacing 15 m (f) Spacing 10 m

Fig. 3 Simulation results of stress distribution of anchored surrounding rock

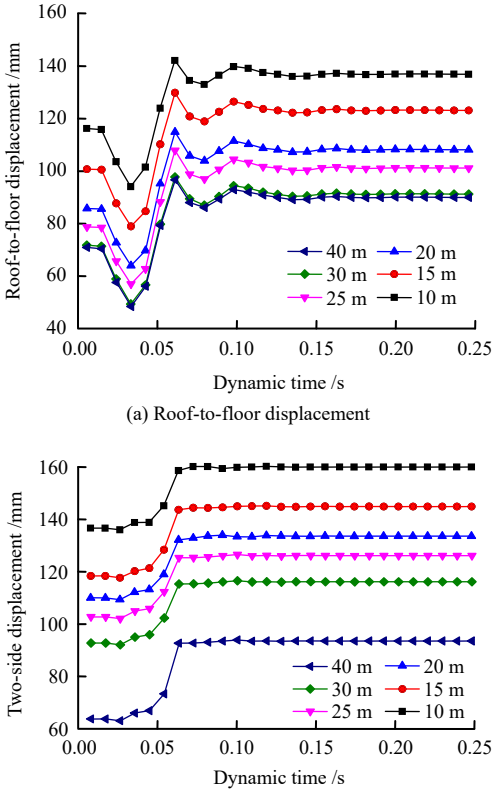

(a) Roof-to-floor displacement

(b) Two-side displacement

Fig. 4 Simulation results of deformation of anchored surrounding rock

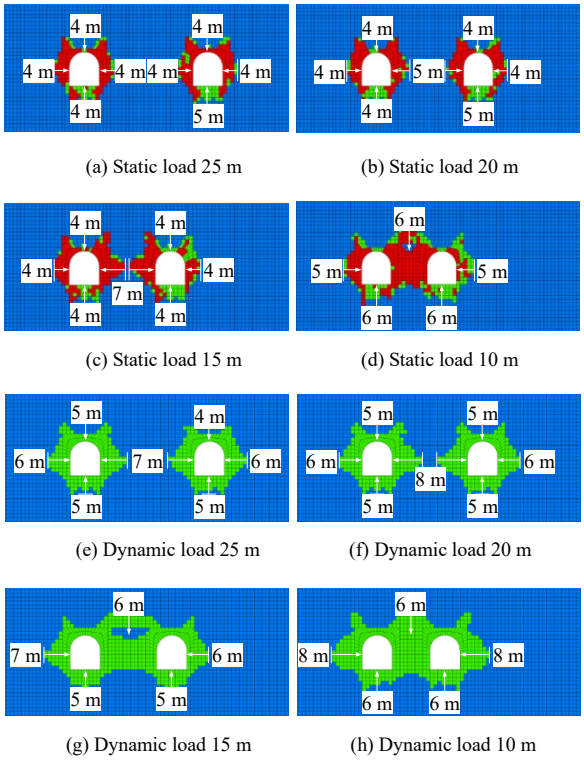

(a) Static load 25 m (b) Static load 20 m

(c) Static load 15 m (d) Static load 10 m

(e) Dynamic load 25 m (f) Dynamic load 20 m

(g) Dynamic load 15 m (h) Dynamic load 10 m

Fig. 5 Simulation results of plastic failure distribution of anchored surrounding rock

Under the static load, when the chamber spacing decreases from 40 m to 30 m, the stress distribution and peak value of the anchored surrounding rock remain unchanged, while the two-side displacement is rather obvious. The plastic zone is developed and the maximum failure depth is 5.0 m. When the chamber spacing decreases

from 25 m to 20 m, the stress peak of surrounding rock increases marginally, the overall deformation of surrounding rock increases slightly, and the plastic failure depth keeps unchanged but the failure area expands. When the chamber spacing continues to decrease to 10 m, the stress peak increases significantly, rising by about 21.3%. The roof-to-floor deformation is evidently increased by 67.2%, and the two-side displacement increases by nearly 1.2 times. In this chamber spacing range (spacing≤15 m), the anchored surrounding rock deformation is serious, and the plastic zones on the sides of adjacent coal(rock) pillars are connected with each other, resulting in the overall chamber failure.

After disturbed by dynamic load, the deformation and failure degree of anchored rock keeps increasing. Compared with chamber spacing of 40 m, when the chamber spacing is 30 m, there are minor increases of the stress peak value and roof-to-floor movement of surrounding rock, and the two-side displacement increases about 33.4%. The maximum failure depth of anchored rock is basically stable and the total failure area increases slightly. When the chamber spacing is reduced to 25−20 m, the stress accumulates rapidly. The roof-to-floor movement increases by about 20.2% and the deformation increases by about 53.4%. As the chamber spacing decreases, the stress of the surrounding rock between chambers is higher than that of the original rock, indicating a mutual influence and stress superposition between them. The plastic failure zone expands to the elastic zone, and the maximum failure depth reaches up to 8.0 m. When the spacing between chambers is 15−10 m, the stress concentration of surrounding rock rises sharply. The deformation and failure of chambers become more severe, and the displacements of roof-to-floor and two sides increase by 52.3% and 83.7%, respectively. As the distance between chambers continues to decrease, the interaction between them is highly enhanced, and the coal (rock) pillars in the middle of the chamber begin to be connected. Furthermore, the elastic core disappears, the degree of failure intensifies, and the plastic failure zone expands to the chamber exterior.

According to the simulation results (Fig.6), prior to being disturbed by dynamic load, both sides of the two chambers are subjected to high stress concentration, and affected by mutual interference. The stress in the coal pillar in the middle of the chambers is superimposed under severe stress concentration, with the maximum stress on one side about 1.0−1.2 times of that on the other side. The critical spacing for the failure of the entire chamber group under static load is between 10 and 15 m. Under the dynamic load, the deformation and failure degree of anchoring rock is further aggravated by the twofold influence of superimposed stress and dynamic load disturbance. When the spacing between chambers is 40−25 m, the superposition of static loading stress gradually appears, the maximum failure depth of surrounding rock increases slightly. The total area of failure zone increases to some extent, and the coal (rock) pillars between chambers possess elastic zone all along. As the chamber spacing decreases to 20−10 m, the stress of inter-chamber surrounding rock increases significantly. Moreover, the superimposed stress becomes stronger, and the degree of plastic failure is aggravated. As a result, the plastic failure zone begins to connect with each other at the wall and roof, until it is completely connected. At this time, the critical spacing range of the chamber group increases to 15−20 m, which increases by 33.3%−50% compared with that under static load.

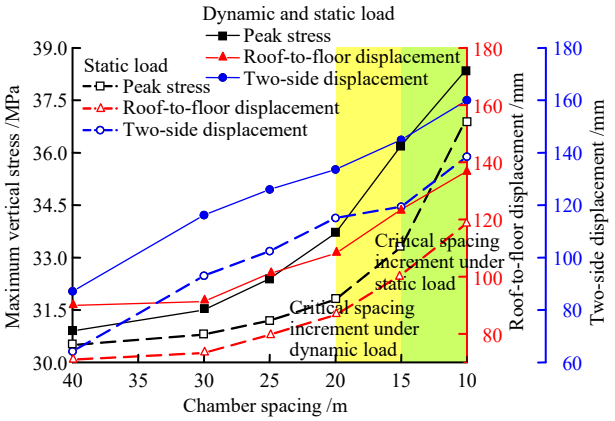

Fig. 6 Comparison of stress and deformation under different spacings

2.2.2 Dynamic load strengths

In order to obtain the influence of dynamic load strength on the stability of surrounding rock of super-large section chamber group, the chamber spacing of 20 m is selected to further explore the dynamic response characteristics under different dynamic load strengths. The vertical stress distribution of chamber surrounding rock is plotted in Fig.7, and the deformations of the roof-to-floor and two sides are plotted in Fig.8. Fig.9 illustrates the distribution of the plastic failure zone of surrounding rock.

For the dynamic load strength of 2.5−3.0 MPa, the stress and deformation degree of surrounding rock are slightly increased. Compared with the dynamic load strength of 2.0 MPa, the deformations of roof-to-floor and

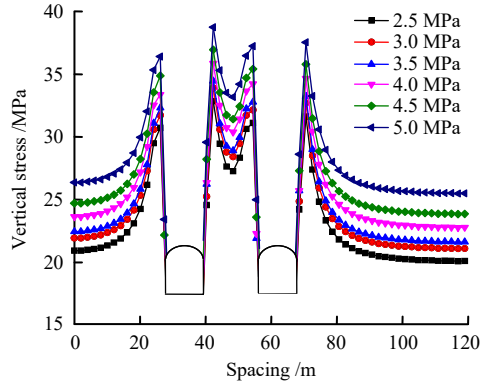

Fig. 7 Stress distribution of anchored surrounding rock under different dynamic load strengths

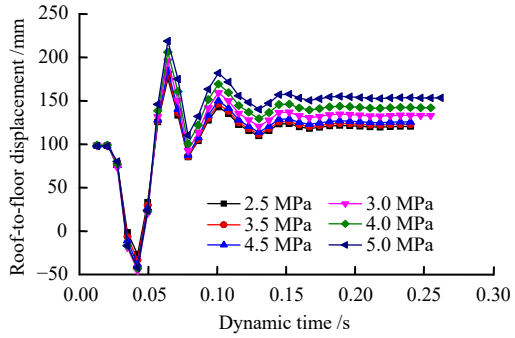

(a) Roof-to-floor displacement

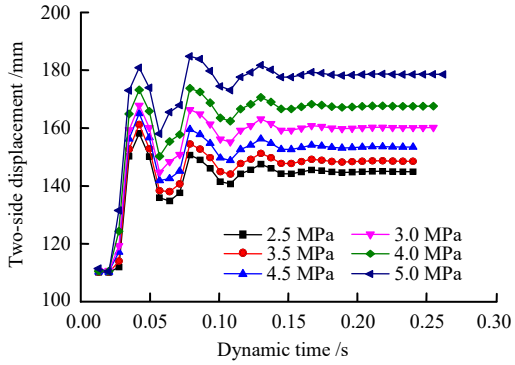

(b) Two-side displacement

Fig. 8 Deformation of anchored surrounding rock under different dynamic load strengths

two sides increase by about 13.6% and 11.2%, respectively. With the increase of dynamic load strength, the plastic failure range and depth are also increased. The maximum failure depth, which is 9.0 m, occurs in the chamber wall. When the dynamic load strength reaches 3.5−4.0 MPa, the stress concentration strengthens markedly along with severe surrounding rock deformation. The roof-to-floor deformation increases by about 23.0%, and the two-side displacement increases by 19.9%. At this point, under the dynamic load, the plastic failure zone of the two sides expands continuously, and the maximum failure depth reaches 10.0 m. When the dynamic load strength goes up to 4.5−5.0 MPa, the deformation of surrounding rock is severe with 41.9% increment of the deformation of roof-to-floor, and 33.6% of the deformation of two sides. The plastic zone expands obviously under such strong dynamic disturbance. For the dynamic load strength of 4.5 MPa, the plastic zone of the anchored surrounding rock breaks through at the wall and then the roof. For the dynamic load strength of 5.0 MPa, the plastic zones between the wall and the roof are all connected and the plastic failure zone is further expanded.

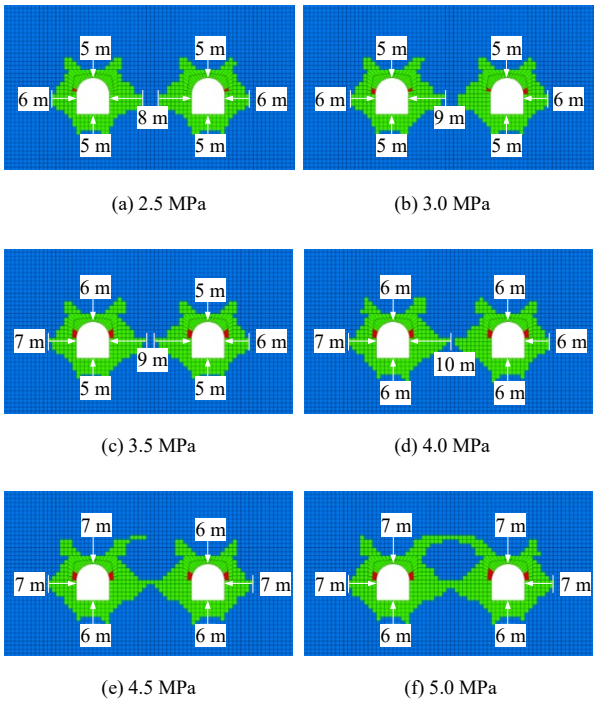

(a) 2.5 MPa (b) 3.0 MPa

(c) 3.5 MPa (d) 4.0 MPa

(e) 4.5 MPa (f) 5.0 MPa

Fig. 9 Plastic failure distribution of anchored surrounding rock under different dynamic strengths

The simulation results highlight that the response of the chamber surrounding rock ratchets up with the increase of dynamic load strength, as reflected in Fig.10. When dynamic load strength is 2.5−3.0 MPa, the influence of dynamic load is insignificant, and the surrounding rock is more intact and stable. As the dynamic load strength continues to increase, the stress of surrounding rock between chambers skyrockets when the dynamic load strength is 4.5−5.0 MPa. The failure degree of surrounding rock is intensified and gradually connected in the wall and roof, and the failure and instability of the chamber group occur under the dynamic load disturbance. Therefore, under the condition of current chamber spacing and section, the critical dynamic load strength range that causes the failure and instability of the anchoring rock is determined as 4.0−4.5 MPa.

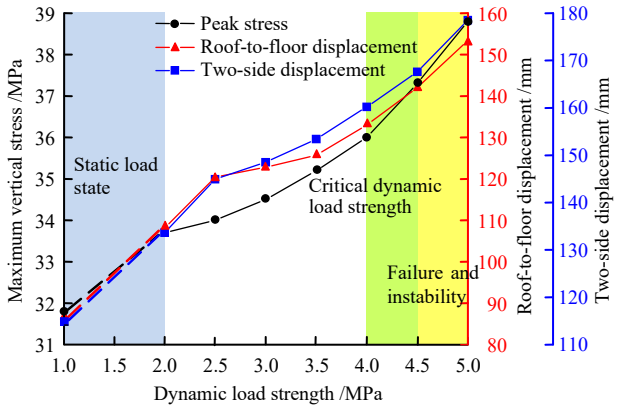

Fig. 10 Comparison of stress and deformation of anchored surrounding rock under different dynamic strengths

3 Failure and instability mechanism of anchored surrounding rock of chamber group

3.1 Failure and instability mechanics criterion

Due to the heterogeneity and anisotropy of surrounding rock in practice, it is difficult to obtain the exact analytical solution. To simplify, the following assumptions are made: (1) The surrounding rock of the chamber is homogeneous and ideal elastic-plastic body; (2) The section of the chamber is round; (3) The dynamic load in underground coal mine is simplified as sinusoidal wave, and the waveform function of the seismic dynamic load intensity σ_D is

$$\sigma_D = \begin{cases} A\sin(2\pi ft) & 0 \leqslant t \leqslant T \\ 0 & t > T \end{cases} \tag{1}$$

where A is the amplitude of dynamic load of seismic source (MPa); f is the frequency (Hz); t is the response time (s); and T is the time period (s).

The failure of chamber anchored bearing structure under dynamic load disturbance involves mechanical evolution driven by static mining load and external dynamic load. When the anchored surrounding rock after excavation stabilization is disturbed by external dynamic load, the rock mass originally in elastic state may exceed its dynamic compressive strength and generate new damage and failure, accompanied by stress concentration and energy accumulation or dissipation. As depicted in Fig.11, the chamber surrounding rock is simultaneously affected by concentrated stress, static load superimposed stress, and external dynamic load disturbance.

In this case, the stress and energy of the surrounding rock under the dynamic load are expressed as

$$\left.\begin{aligned} \sigma_w &= \sigma_j + \Delta\sigma_j + \Delta\sigma_d \\ U_y &= U_0 + \Delta U_j + \Delta U_d - U_i \end{aligned}\right\} \tag{2}$$

where σ_w is the stress of chamber anchored surrounding rock (MPa); σ_j is the concentrated stress (MPa); $\Delta\sigma_j$ is the static load superimposed stress increment (MPa); $\Delta\sigma_d$ is the external dynamic load stress increment (MPa); U_0 is the elastic strain energy that initially accumulated in surrounding rock (kJ); ΔU_j is the increment of elastic energy by static loading superimposed stress (kJ); ΔU_d is the accumulation of elastic energy by external dynamic load disturbance (kJ); U_i is the energy consumed by deformation and failure of supporting structure (kJ); and U_y is the elastic complementary energy (kJ).

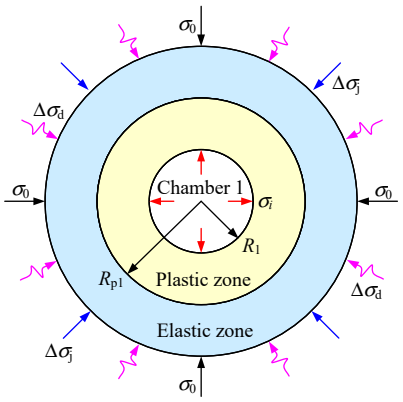

Fig. 11 Mechanical model of anchored surrounding rock under dynamic and static loads

According to the theory of elastic-plastic mechanics, the stress field of surrounding rock is redistributed after excavation of Chamber 1, which is divided into plastic zone (radius is R_{p1}) and elastic zone. The concentrated stress in the elastic zone σ_j is

$$\left.\begin{aligned} \sigma_j^{\theta} &= \sigma_0\left[1+\left(\frac{R_1}{l_1}\right)^2\right] - \sigma_i\left(\frac{R_1}{l_1}\right)^2 \\ \sigma_j^{z} &= \sigma_0 \\ \sigma_j^{r} &= \sigma_0\left[1-\left(\frac{R_1}{l_1}\right)^2\right] + \sigma_i\left(\frac{R_1}{l_1}\right)^2 \end{aligned}\right\} \tag{3}$$

where R_1 is the radius of Chamber 1 (m); l_1 is the distance between a point in the elastic zone and the center of Chamber 1 (m); and σ_i is the support resistance of the anchored surrounding rock in Chamber 1 (MPa).

The increment of static stress induced by the excavation of Chamber 2 $\Delta\sigma_j$ is

$$\Delta\sigma_{\mathrm{j}}=\sigma_0\left[1+\left(\frac{R_2}{l_2}\right)^2\right]-\sigma_{\mathrm{i}}'\left(\frac{R_2}{l_2}\right)^2-\sigma_0=$$

$$(\sigma_0-\sigma_{\mathrm{i}}')\left(\frac{R_2}{l_2}\right)^2 \tag{4}$$

where R_2 is the radius of Chamber 2 (m); σ_{i}' is the support resistance of the anchored surrounding rock in Chamber 2 (MPa); and l_2 denotes the distance between a point in the elastic zone and the center of Chamber 2 (m).

According to the theory of elastic wave propagation, the stress wave under dynamic load will attenuate as it propagates to the vicinity of the chamber due to the interference and reflection phenomena. Under the circumstances, the increment of dynamic load applied to the anchored surrounding rock $\Delta\sigma_{\mathrm{d}}$ is

$$\Delta\sigma_{\mathrm{d}}=\sigma_{\mathrm{D}}\mathrm{e}^{-\lambda_{\mathrm{E}}L} \tag{5}$$

where λ_{E} is the stress attenuation coefficient (m^{-1}); and L is the distance between the dynamic load source and the chamber (m).

Substituting Eqs. (3)−(5) into Eq.(2), the following Eq.(6) is obtained.

$$\sigma_{\mathrm{w}}=\sigma_0\left[1+\left(\frac{R_1}{l_1}\right)^2\right]-\sigma_{\mathrm{i}}\left(\frac{R_1}{l_1}\right)^2+$$

$$(\sigma_0-\sigma_{\mathrm{i}}')\frac{R_2^2}{l_2^2}+\sigma_{\mathrm{D}}\mathrm{e}^{-\lambda_{\mathrm{E}}L} \tag{6}$$

The elastic energy U_{j} released per unit volume of coal under static load is

$$U_{\mathrm{j}}=\frac{\sigma_1^2+\sigma_2^2+\sigma_3^2-2\mu\left(\sigma_1\sigma_2+\sigma_1\sigma_3+\sigma_2\sigma_3\right)}{2E_{\mathrm{m}}} \tag{7}$$

where E_{m} and μ are the elasticity modulus and Poisson's ratio of the surrounding rock, respectively.

Substituting Eq.(3) into Eq.(7) gives

$$U_0=\frac{3\sigma_0^2\left(1-2\mu\right)}{2E_{\mathrm{m}}}+\frac{\left(1+\mu\right)\left(\sigma_0-\sigma_{\mathrm{i}}\right)^2R_1^4}{E_{\mathrm{m}}l_1^4} \tag{8}$$

According to the theory of minimum energy, the elastic energy increment generated by excavation of Chamber 2 and the energy accumulated by external dynamic load disturbance are

$$\left.\begin{aligned}\Delta U_{\mathrm{j}}&=\frac{\Delta\sigma_{\mathrm{j}}^2}{2E_{\mathrm{m}}}=\frac{\left(\sigma_0-\sigma_{\mathrm{i}}'\right)^2R_2^4}{2E_{\mathrm{m}}l_2^4}\\ \Delta U_{\mathrm{d}}&=\frac{\Delta\sigma_{\mathrm{d}}^2}{2E_{\mathrm{m}}}=\frac{\sigma_{\mathrm{D}}^2\mathrm{e}^{-2\lambda_{\mathrm{E}}L}}{2E_{\mathrm{m}}}\end{aligned}\right\} \tag{9}$$

Anchor bolts and cables are installed in fixed spacing along the periphery of the circular chamber. The compression zone of the cone formed under the prestress overlaps and connects with each other, forming a continuous bearing structure within the surrounding rock. The energy consumed for deformation and failure of the structure under dynamic and static superimposed stress is

$$U_{\mathrm{i}}=\frac{\sigma_{\mathrm{i}}^2}{2E_{\mathrm{m}}}=\frac{\left(n_{\mathrm{s}}Q_{\mathrm{s}}+n_{\mathrm{g}}Q_{\mathrm{g}}\right)^2}{8E_{\mathrm{m}}\pi^2R_1^2} \tag{10}$$

where Q_{g} is the maximum axial force of bolt (kN); n_{g} is the number of bolts; Q_{s} is the maximum axial force of anchor cable (kN); and n_{s} is the number of cables.

By substituting Eqs. (8)–(10) into Eq.(2), the following Eq.(11) is obtained.

$$U_{\mathrm{y}}=\frac{3\sigma_0^2\left(1-2\mu\right)}{2E_{\mathrm{m}}}+\frac{\left(1+\mu\right)\left(\sigma_0-\sigma_{\mathrm{i}}\right)^2R_1^4}{E_{\mathrm{m}}l_1^4}+$$

$$\frac{\left(\sigma_0-\sigma_{\mathrm{i}}'\right)^2R_2^4}{2E_{\mathrm{m}}l_2^4}+\frac{\sigma_{\mathrm{D}}^2\mathrm{e}^{-2\lambda_{\mathrm{E}}L}}{2E_{\mathrm{m}}}-\frac{\left(n_{\mathrm{s}}Q_{\mathrm{s}}+n_{\mathrm{g}}Q_{\mathrm{g}}\right)^2}{8E_{\mathrm{m}}\pi^2R_1^2} \tag{11}$$

Dynamic compressive strength of rock is commonly adopted as a key index to evaluate the ability to resist dynamic disturbance[39]. Based on the above analysis, when $\sigma_{\mathrm{w}}\leqslant\sigma_{\mathrm{st}}$ and $U_{\mathrm{y}}\leqslant0$, i.e. when the static and dynamic superimposed stress is less than the dynamic compressive strength of the surrounding rock, there is no elastic complementary energy, no new damage occurs under the protection of supporting structure. The deformation of the supporting structure is within the tolerable range, and the entire anchored surrounding rock is in the energy stable state.

When $\sigma_{\mathrm{w}}>\sigma_{\mathrm{st}}$ and $U_{\mathrm{y}}\leqslant0$, i.e. when the static and dynamic superimposed stress exceeds the dynamic compressive strength, there is no elastic complementary energy, the support resistance provided by the anchoring bearing structure is less than the static and dynamic superimposed stress. The energy absorption magnitude of the support structure is greater than the sum of the external accumulated energy, in which case the chamber is determined to be in a static and stable failure state.

When $\sigma_{\mathrm{w}}>\sigma_{\mathrm{st}}$ and $U_{\mathrm{y}}>0$, i.e. when the static and dynamic superimposed stress is greater than the dynamic load strength, the elastic complementary energy exists, the sum of the increment of concentrated stress, static superimposed stress and dynamic disturbed stress is larger than the dynamic compressive strength of the anchored rock mass, the stress limit equilibrium state is broken and the plastic caving failure appears. Meanwhile, the sum

of the released elastic strain energy, static load and dynamic load disturbance energy is more than the energy consumption of deformation and failure of supporting structure. In other words, there is elastic complementary energy stored in the chamber surrounding rock, which can be converted into kinetic energy and mechanical energy, leading to a dynamic failure and instability of the deep rock mass. Thus, the failure and instability criterion of the chamber can be determined as

$$\left.\begin{array}{ll}\sigma_{\mathrm{w}} \leqslant \sigma_{\mathrm{st}},\ U_{\mathrm{y}} \leqslant 0 & \text{Overall stability}\\ \sigma_{\mathrm{w}} > \sigma_{\mathrm{st}} \begin{cases} U_{\mathrm{y}} \leqslant 0, & \text{Static failure}\\ U_{\mathrm{y}} > 0, & \text{Dynamic instability}\end{cases}\end{array}\right\} \tag{12}$$

3.2 Engineering application and validation

The above theoretical analysis and numerical simulation are applied to Longgu Coal Mine screening product transfer chamber and slime water and medium chamber for case study. When the stress exceeds the dynamic compressive strength of the anchored rock and there is elastic complementary energy, chamber dynamic instability occurs. At this point, a limit state exists, which satisfies,

$$\left.\begin{array}{l}\sigma_{\mathrm{w}} = 0\\ U_{\mathrm{y}} = 0\end{array}\right\} \tag{13}$$

Combining Eqs. (2), (6) with Eqs. (11), (13) yields

$$\left.\begin{array}{l}\sigma_0\left[1+\left(\dfrac{R_1}{l_1}\right)^2\right]-\sigma_{\mathrm{i}}\left(\dfrac{R_1}{l_1}\right)^2+(\sigma_0-\sigma_{\mathrm{i}}')\dfrac{R_2^2}{l_2^2}+\sigma_{\mathrm{D}}\mathrm{e}^{-\lambda_{\mathrm{E}}L}-\\ \sigma_{\mathrm{st}}=0\\ \dfrac{3\sigma_0^2(1-2\mu)}{2E_{\mathrm{m}}}+\dfrac{(1+\mu)(\sigma_0-\sigma_{\mathrm{i}})^2R_1^4}{E_{\mathrm{m}}l_1^4}+\dfrac{(\sigma_0-\sigma_{\mathrm{i}}')^2R_2^4}{2E_{\mathrm{m}}l_2^4}+\\ \dfrac{\sigma_{\mathrm{D}}^2\mathrm{e}^{-2\lambda_{\mathrm{E}}L}}{2E_{\mathrm{m}}}-\dfrac{(n_{\mathrm{s}}Q_{\mathrm{s}}+n_{\mathrm{g}}Q_{\mathrm{g}})^2}{8E_{\mathrm{m}}\pi^2R_1^2}=0\end{array}\right\} \tag{14}$$

l_1 and l_2 can be obtained by solving Eq.(14), and the critical spacing L for chamber instability can be determined as

$$L = l_1 + l_2 \tag{15}$$

The equivalent radius method is used to correct the on-site chamber,

$$R_0 = K(S/\pi)^{1/2} \tag{16}$$

where S is the actual chamber section area (m^2); and K is the section correction coefficient of arched chamber, set as 1.1[40]. By referring to rock mechanics laboratory test, on-site chamber support scheme, field stress measurement and microseismic data, the parameters are assessed as summarized in Table 3. By combining Eq.(14) and Eq.(16), the anchored surrounding rock of the on-site chamber meets the following conditions:

$$\left.\begin{array}{l}\dfrac{SK^2}{\pi l_1^2}+\dfrac{SK^2}{\pi l_2^2}=\dfrac{\sigma_{\mathrm{st}}-\sigma_0-\sigma_{\mathrm{d}}}{\sigma_0-\sigma_{\mathrm{i}}}\\ 2(1+\mu)\left(\dfrac{SK^2}{\pi l_1^2}\right)^2+\left(\dfrac{SK^2}{\pi l_2^2}\right)^2=\\ \dfrac{(n_{\mathrm{s}}Q_{\mathrm{s}}+n_{\mathrm{g}}Q_{\mathrm{g}})^2}{4\pi SK^2}-\sigma_{\mathrm{d}}^2-3\sigma_0^2(1-2\mu)\\ \qquad\qquad (\sigma_0-\sigma_{\mathrm{i}})^2\end{array}\right\} \tag{17}$$

Table 3 Parameter selection of calculation example[41−42]

Parameter	S	σ_0	σ_{st}	λ_{E}	L	E_{m}	μ	n_{g}	Q_{g}	n_{s}	Q_{s}
Value	65.1	20.0	150.0	2.5×10^{-2}	60.0	40.0	0.2	17	190	9	654

Field monitoring suggests that $\sigma_{\mathrm{i}} = 0.3$ MPa and $\sigma_{\mathrm{d}} =$ 0−5.0 MPa. Substituting them into Eq.(17), the relationship curve between the critical spacing of the chamber and dynamic load strength is obtained, as shown in Fig.12. With the increase of dynamic load strength, the critical spacing between chambers increases and the range of failure and instability is enlarged. The fitting analysis shows a quadratic function relationship between dynamic load strength and critical spacing of chamber group with an excellent fitting effect ($R^2 \approx 0.99$). The fitting equation is written as

$$L = 0.25\sigma_{\mathrm{d}}^2 + 1.01\sigma_{\mathrm{d}} + 8.82 \tag{18}$$

Substituting the minimum field spacing of chambers (15 m) into Eq.(18), it is found that under the given geological and engineering conditions, dynamic load with

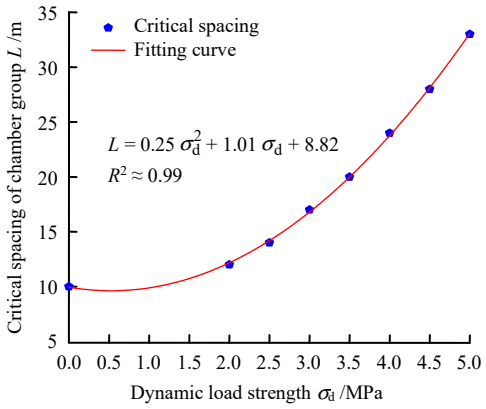

Fig. 12 Relationship between chamber critical spacing and dynamic load strength

strength below 3.34 MPa has little influence on the chamber group, and thus there seems no risk of failure and instability. However, when the dynamic load strength reaches 5.0 MPa, the critical spacing of the chamber group is 33.0 m, and the failure and instability range of the on-site chamber group would exceed 69%. Hence, it is imperative to apply the corresponding reinforcement measures in a certain range to improve the anti-seismic and energy absorption characteristics of surrounding rock so as to ensure the overall stability of the chamber group.

The research group conducted a follow-up survey on the coal gangue separation chamber group, and monitored the surrounding rock deformation of the screening product transfer chamber and slime water and medium chamber, as shown in Fig.13. It was found that about 95% of the displacement occurred within 100 days after excavation, and gradually stabilized after 120 days. The maximum roof-to-floor displacement and two-side displacement of the screening product transfer chamber were 107 mm and 75 mm, and the maximum roof-to-floor displacement and two-side displacement of the slime water and medium chamber were 125 mm and 87 mm, respectively. The field monitoring data manifests an advantageous performance on field application that the surrounding rock of the chamber group remains overall stable, as shown in Fig.14.

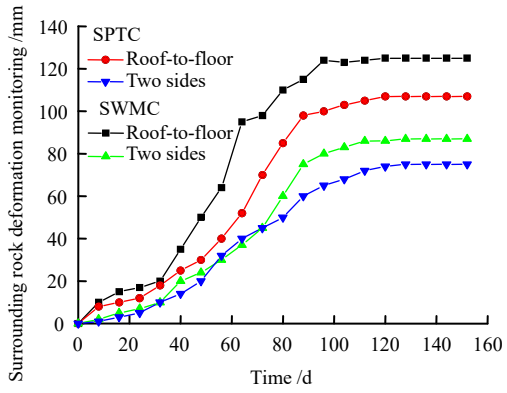

Fig. 13 Deformation monitoring of surrounding rock of chambers

(a) SPTC (b) SWMC

Fig. 14 Field application of chambers

4 Conclusions

(1) The surrounding rock of deep super-large section chamber group is affected by the superimposed stress and dynamic load. It is characterized by large deformation and failure range, and the failure evolution is closely related to the chamber spacing and dynamic load strength. With the decrease of chamber spacing, the deformation and failure degree of surrounding rock gradually increase, resulting in the overall failure and instability. Compared with the static load, the critical spacing of the chamber group under dynamic load increases by 33.3%−50%, reaching 15−20 m. With the increase of dynamic load strength, the response of anchoring surrounding rock gradually increases, and the critical dynamic load strength for failure and instability is approximately 4.0−4.5 MPa.

(2) The mechanical model of anchored surrounding rock under dynamic and static superposed load is established to reveal the stress and energy evolution characteristics of surrounding rock under the influence of concentrated stress, static load superposition and external dynamic load disturbance. The failure and instability criterion of the anchored surrounding rock of deep chamber group under dynamic load is obtained, which can be divided into three states: overall stability, static failure and dynamic instability. Based on the absence of dynamic instability, the analytical expression of critical spacing for failure and instability of chamber group is derived.

(3) According to the geological conditions of the screening product transfer chamber and the slime water and medium chamber in Longgu Coal Mine, by using the equivalent radius method, it is found that the critical spacing of the chamber groups in failure and instability state increases in a quadratic function with increasing the dynamic load strength. Under the site-specific condition, the anchored surrounding rock commences to be affected by the external dynamic load disturbance when the dynamic load strength surpasses 3.34 MPa. Therefore, it is necessary to carry out reinforcement supports to ensure the overall stability of chamber surrounding rock. The research results can provide theoretical basis for the design of deep dynamic load chambers and stability control of surrounding rock under the similar conditions.

References

[1] TAN Yun-liang, FAN De-yuan, LIU Xue-sheng, et al. Discrimination method and engineering characteristics of

super large section chamber in coal mine[J]. Journal of Mining & Safety Engineering, 2020, 37(1): 23−31.

[2] YUAN Yong, YUAN Chao-feng, ZHU Cheng, et al. Mechanical model and application of the deformation cylinder of the surrounding rock in the deep large section chamber[J]. Journal of Mining & Safety Engineering, 2020, 37(2): 338−348.

[3] LIU Xue-sheng, TAN Yun-liang, NING Jian-guo, et al. Energy criterion of abutment pressure induced strain-mode rockburst[J]. Rock and Soil Mechanics, 2016, 37(10): 2929−2936.

[4] KANG Hong-pu, WANG Jin-hua, LIN Jian. Case studies of rock bolting in coal mine roadways[J]. Chinese Journal of Rock Mechanics and Engineering, 2010, 29(4): 649−664.

[5] ZHU Cheng, YUAN Yong, YUAN Chao-feng, et al. Stability evaluation and layout of surrounding rock in deep large section tunnel[J]. Journal of Mining & Safety Engineering, 2020, 37(1): 11−22.

[6] NING Jian-guo, QIU Peng-qi, YANG Shu-hao, et al. Damage mechanism and support of surrounding rock anchorage structure of deep large section chamber under static-dynamic coupling loading[J]. Journal of Mining & Safety Engineering, 2020, 37(1): 50−61.

[7] HE Man-chao. Progress and challenges of soft rock engineering in depth[J]. Journal of China Coal Society, 2014, 39(8): 1409−1417.

[8] XIE He-ping, GAO Feng, JU Yang. Research and development of rock mechanics in deep ground engineering[J]. Chinese Journal of Rock Mechanics and Engineering, 2015, 34(11): 2161−2178.

[9] TAN Yun-liang, GUO Wei-yao, XIN Heng-qi, et al. Key technology of rock burst monitoring and control in deep coal mining[J]. Journal of China Coal Society, 2019, 44(1): 160−172.

[10] LIU Xue-sheng, TAN Yun-liang, NING Jian-guo. Chaotic prediction of surrounding rock deformation speed in coal roadway supported by bolt[J]. Journal of Mining & Safety Engineering, 2014, 31(3): 385−389.

[11] CONG Li, CAO An-ye, ZHOU Yuan-hong, et al. The comprehensive pre-warning method of rock burst hazard based on theory of dynamic and static combined loading[J]. Journal of Mining & Safety Engineering, 2020, 37(4): 767−776.

[12] YUAN Liang, JIANG Yao-dong, HE Xue-qiu, et al. Research progress of precise risk accurate identification and monitoring early warning on typical dynamic disasters in coal mine[J]. Journal of China Coal Society, 2018, 43(2): 306−318.

[13] DOU Lin-ming, LI Zhen-lei, ZHANG Min. Study on monitoring and early warning technology of mine pressure bump disaster[J]. Coal Science and Technology, 2016, 44(7): 41−46.

[14] GAO Ming-shi, ZHANG Nong, DOU Lin-ming, et al. Study of roadway support parameters subjected to rock burst based on energy balance theory[J]. Journal of China University of Mining & Technology, 2007, 36(4): 426−430.

[15] QIAN Qi-hu, QI Cheng-zhi. Dynamic strength and dynamic fracture criteria of rock and rock mass[J]. Journal of Tongji University (Natural Science), 2008, 36(12): 1599−1605.

[16] LIU Shao-hong. Nonlinear catastrophy model and chaotic dynamic mechanism of compound coal-rock unstable failure under coupled staticdynamic loading[J]. Journal of China Coal Society, 2014, 39(2): 292−300.

[17] LIU Dong-qiao, HE Man-chao, WANG Cheng-chao, et al. Experimental study on rock burst induced by dynamic load[J]. Journal of China Coal Society, 2016, 41(5): 1099−1105.

[18] WANG Bin, LI Xi-bing, MA Chun-de, et al. Principle and preliminary application of combined static-dynamic support to rockburst disaster controlling[J]. Chinese Journal of Rock Mechanics and Engineering, 2014, 33(6): 1169−1178.

[19] LIU Xue-sheng. Study on the mechanism and control of rockburst in roadways under dynamic loads[D]. Qingdao: Shandong University of Science and Technology, 2017.

[20] LI Di-yuan, CHENG Teng-jiao, ZHOU Tao, et al. Experimental study of the dynamic strength and fracturing characteristics of marble specimens with a single hole under impact loading[J]. Chinese Journal of Rock Mechanics and Engineering, 2015, 34(2): 249−260.

[21] LIU Xue-sheng, SONG Shi-lin, FAN De-yuan, et al. Experimental study on deformation and failure evolution of surrounding rock for deep super-large section chamber group[J]. Journal of Mining & Safety Engineering, 2020, 37(1): 40−49.

[22] PAN Yi-shan, LÜ Xiang-feng, LI Zhong-hua, et al. Experimental study of dynamic failure process of roadway under high velocity impact loading[J]. Rock and Soil Mechanics, 2011, 32(5): 1281−1286.

[23] WANG Si-wei, LIU Han-dong, JIANG Tong. Large geomechanical model test on failure mechanism of rockburst tunnel under static and explosive loads[J]. Chinese Journal of Rock Mechanics and Engineering, 2014, 33(10): 2095−2100.

[24] ZUO Yu-jun, MA Chun-de, ZHU Wan-cheng, et al. Model test study of mechanism of layered fracture within surrounding

rock of tunnels in deep stratum tunnelling under dynamic disturbance[J]. Rock and Soil Mechanics, 2011, 32(10): 2929−2936.

[25] LIU Shao-hong, MAO De-bing, QI Qing-xin, et al. Under static loading stress wave propagation mechanism and energy dissipation in compound coal-rock[J]. Journal of China Coal Society, 2014, 39(Suppl.1): 15−22.

[26] XIE Long, DOU Lin-ming, LÜ Chang-guo, et al. Study on the effect of floor burst induced by dynamic disturbance at different lateral pressure coefficients[J]. Journal of Mining & Safety Engineering, 2013, 30(2): 251−255.

[27] ZHANG Ming, JIANG Fu-xing, CHEN Guang-yao, et al. A stope stress transfer model based on the motion state of thick and hard rock strata and its application[J]. Chinese Journal of Rock Mechanics and Engineering, 2020, 39(7): 1396−1407.

[28] XIAO Zhi-min, LIU Jun, WANG He, et al. Study on mechanism and control of rock burst instability of roadway floor induced by dynamic load disturbance[J]. Chinese Journal of Underground Space and Engineering, 2019, 15(5): 1573−1581.

[29] XIAO Tong-qiang, LI Hua-min, YANG Jian-li, et al. Deformation and failure mechanism of surrounding rock in chamber with super large section and its control[J]. Journal of China Coal Society, 2014, 39(4): 631−636.

[30] SUN Xiao-ming, WANG Dong, MIAO Cheng-yu, et al. Research on dynamic pressure instability mechanism and control countermeasure of deep pump room and chamber group in nantun coal mine[J]. Journal of China Coal Society, 2015, 40(10): 2303−2312.

[31] JIANG Xin, DU Hai-wen, YUAN Xuan, et al. Study on early warning of safety risk in underground cavern group construction under neural network paradigm[J]. China Safety Science Journal, 2018, 28(2): 181−186.

[32] KANG Hong-pu. Spatial scale analysis on coal mining and strata control technologies[J]. Journal of Mining and Strata Control Engineering, 2020, 2(2): 5−30.

[33] HE Man-chao, LI Guo-feng, REN Ai-wu, et al. Analysis of the stability of intersecting chambers in deep soft-rock roadway construction[J]. Journal of China University of Mining & Technology, 2008, 37(2): 167−170.

[34] YANG Ren-shu, XUE Hua-jun, GUO Dong-ming, et al. Failure mechanism of surrounding rock of large section chambers in complex rock formations and its control[J]. Journal of China Coal Society, 2015, 40(10): 2234−2242.

[35] WANG Qi-zhou, XIE Wen-bing, JING Sheng-guo, et al. Instability mechanism and control technology of chamber group surrounding rock in complex structural area[J]. Journal of Mining & Safety Engineering, 2014, 31(2): 263−269.

[36] TAN Yun-liang, FAN De-yuan, LIU Xue-sheng, et al. Numerical investigation on failure evolution of surrounding rock for super-large section chamber group in deep coal mine[J]. Energy Science and Engineering, 2019, 7: 3124−3146.

[37] LIU Xue-sheng, WU Yun-hao, TAN Yun-liang, et al. Influence of bolt fatigue resistance on the surrounding rock stability of deep chamber disturbed by dynamic loads[J]. Journal of China University of Mining & Technology, 2021, 50(3): 449−458.

[38] WU Yong-zheng, CHEN Jin-yu, JIAO Jian-kang, et al. Damage and failure mechanism of anchored surrounding rock with impact loading[J]. Journal of China Coal Society, 2018, 43(9): 2389−2397.

[39] NING Jian-guo. Rock mechanics[M]. Beijing: China Coal Industry Publishing House, 2014.

[40] LIU Chang-wu, CAO Lei, LIU Shu-xin. Method of "equivalent radius" for the analyzing rock stress of high-buried non-circular underground chambers[J]. Copper Engineering, 2010(1): 1−5.

[41] DU Bin-bin, WANG Shao-bo, WANG De-jian, et al. Study on numerical simulation of seismic wave transmission law in coal and rock mass[J]. Coal Science and Technology, 2014, 42(Suppl.1): 7−12.

[42] WANG Guan-shi, LI Chang-hong, HU Shi-li, et al. A study of time-and spatial-attenuation of stress wave amplitude in rock mass[J]. Rock and Soil Mechanics, 2010, 31(11): 3487−3492.